Acta Crystallographica Section D
Biological Crystallography
ISSN 0907-4449

Structures of NAD^+- and NADH-bound 1-L-*myo*-inositol 1-phosphate synthase

Xiangshu Jin and James H. Geiger*

Department of Chemistry, Michigan State University, USA

Correspondence e-mail: geiger@cem.msu.edu

Received 15 January 2003
Accepted 10 April 2003

PDB References: 1-L-*myo*-inositol 1-phosphate synthase, apo form, 1p1f, r1p1fsf; NAD^+ bound, $P2_1$, 1p1h, r1p1hsf; NAD^+ bound, $C2$, 1p1i, r1p1isf; NADH bound, 1p1j, r1p1jsf; NADH and EDTA bound, 1p1k, r1p1ksf.

1-L-*myo*-Inositol 1-phosphate synthase catalyzes the conversion of D-glucose 6-phosphate to 1-L-*myo*-inositol 1-phosphate, the first and rate-limiting step in the biosynthesis of all inositol-containing compounds. It involves an oxidation, an intramolecular aldol cyclization and a reduction. Here, the structure of the enzyme in its NAD^+-bound, NADH-bound and apo forms is presented. These structures confirm that a significant portion of the active site is disordered in the absence of a small molecule, as none of the NAD^+-bound forms of the enzyme have ordered active sites. On the other hand, the NADH-bound form contains two small molecules in the active site: a phosphate and glycerol. The entire active site is ordered in the presence of these two molecules, completely encapsulating them within the interior cavity. Significant changes in the structure of the active site are also seen, including repositioning of the nicotinamide ring and a motion of a loop region to accommodate the bound phosphate. These changes call into question the mechanism previously proposed for the enzyme. A comparison of the yeast and mycobacterial enzymes shows a surprisingly large change in the relative orientation of the catalytic and Rossmann-fold domains in the two enzymes.

1. Introduction

Inositol-containing compounds play critical and diverse biological roles including signal transduction, second messenger signaling, stress response and cell-wall biogenesis (Arganoff & Fisher, 1991; Exton, 1986; Majumder *et al.*, 1997; Potter & Lampe, 1995). The biosynthesis of inositol follows a common pathway involving first the conversion of D-glucose 6-phosphate to 1-L-*myo*-inositol 1-phosphate (MIP) catalyzed by MIP synthase, followed by dephosphorylation catalyzed by *myo*-inositol (MI) monophosphatase (Majumder *et al.*, 1997). The synthesis of MIP is both the first committed and the rate-limiting step in this pathway (Majumder *et al.*, 1997). Significant biosynthesis of inositol has been detected in organs where a significant blood barrier exists, such as the testes or brain (Adhikari & Majumder, 1983, 1988; Hasegawa & Eisenberg, 1981; Mauck *et al.*, 1980; Wong *et al.*, 1982). Significantly, reduction of the brain inositol pool by inhibition of MIP phosphatase has been suggested to be the mode of action of lithium in the treatment of bipolar disorder (Belmaker *et al.*, 1995, 1996; Berridge *et al.*, 1982, 1989). Recent *in vivo* results in yeast suggest that Valproate, a drug used in the treatment of depression, bipolar disorder and seizure disorder, may act by inhibition of MIP synthase, thus lowering neuronal inositol pools similar to the action of lithium (Vaden *et al.*, 2001). Regulation of inositol biosynthesis itself may play an important role in the regulation of second messenger signalling.

MIP synthase has been characterized and cloned from a diversity of organisms, including yeast, plants, flies, human, Archaebacteria and Eubacteria (Abu-Abied & Holland, 1994; Chen *et al.*, 2000; Dean-Johnson & Henry, 1989; Ishitani *et al.*, 1996; Johnson, 1994; Johnson & Sussex, 1995; Lohia *et al.*, 1999; Majumder *et al.*, 1997; Park *et al.*, 2000; Smart & Fleming, 1996; Wang & Johnson, 1995). The eukaryotic enzymes are remarkably conserved throughout their length, with better than 45% identity from yeast to flies (Majumder *et al.*, 1997). In all cases the enzyme displays modest catalytic activity, with turnover numbers ranging from 3 to 13 $\mu M\ min^{-1}$ per milligram of enzyme and substrate K_M values in the 100 μM–1 mM range (Chen *et al.*, 2000; Majumder *et al.*, 1997). A significant collection of both biochemical and chemical data have coalesced to the reaction path first proposed by Loewus and colleagues (Fig. 1) (Frey, 1987; Loewus & Kelly, 1962; Loewus & Loewus, 1980; Majumder *et al.*, 1997; Migaud & Frost, 1995). Several inhibitor studies are consistent with the idea that the enzyme first binds the open acyclic tautomer of the substrate D-glucose 6-phosphate, followed by oxidation to the C5 keto intermediate (intermediate *B* in Fig. 1; Tian *et al.*, 1999). Frost and coworkers propose that enolization is promoted by proton extraction *via* the substrate phosphate, consistent with the phosphate binding in a *transoid* conformation (Tian *et al.*, 1999). Intramolecular aldol cyclization followed by re-reduction of the C5 ketone completes the formation of the product. None of the intermediates have been isolated or trapped, suggesting that all intermediates are tightly bound and not released until the final reduction to *myo*-inositol 1-phosphate (Barnett & Corina, 1968; Loewus, 1977; Sherman *et al.*, 1969). The enzyme thus catalyzes three distinct steps: an oxidation, an intramolecular aldol cyclization and finally a reduction, in the same active site with no apparent dissociation of intermediates.

Major questions still remain regarding the mechanism of this enzyme, especially regarding the nature of the aldol cyclization. Typically, enzymes that utilize an aldol cyclization reaction can be categorized as either a type I or type II aldolase. Biochemical data suggest that *Saccharomyces cerevisiae* MIP synthase is neither a type I aldolase, which involves a covalent Schiff base intermediate, nor a type II aldolase, which involves a divalent cation such as zinc or manganese acting as a Lewis acid (Loewus & Loewus, 1973; Mauck *et al.*, 1980; Pittner & Hoffmann-Ostenhof, 1976, 1978; Sherman *et al.*, 1981). Instead, the enzyme is activated fivefold by ammonium ions (Chen *et al.*, 2000). On the other hand, MIP synthase from *Archaeoglobus fulgidus* requires divalent cations and therefore is thought to be a type II aldolase. This is quite surprising considering the high sequence homology between the enzymes (53% similarity; Chen *et al.*, 2000). It is far more common to find enzymes with completely divergent sequences and even completely different three-dimensional structures using identical mechanisms than the converse.

Crystal structures of several MIP synthase enzymes have recently been determined, including MIP synthase from *S. cerevisiae* (yMIP synthase) partially occupied with NAD^+ and bound to fully occupied NAD^+ and an inhibitor, 2-deoxy-D-glucitol 6-phosphate (dgtolP; Stein & Geiger, 2002). While fully 60 residues (351–409) were found to be disordered in the former structure, all of these residues became ordered upon full NAD^+ occupancy and inhibitor binding. The result was complete encapsulation of the inhibitor within a buried active-site cavity, with access completely prevented. It thus appeared that complete folding of the enzyme's active site required complete NAD^+ occupancy, inhibitor/substrate binding, or both. The inhibitor appeared to be bound in a relatively extended conformation inconsistent with intramolecular aldol cyclization. Based on this data, a conformation that would be consistent with the cyclization was modeled and a mechanism for the transformation proposed. In addition, a possible location for the ammonium ion was identified and it was proposed that the ammonium ion performed a similar function to that of a divalent cation in type II aldolases, stabi-

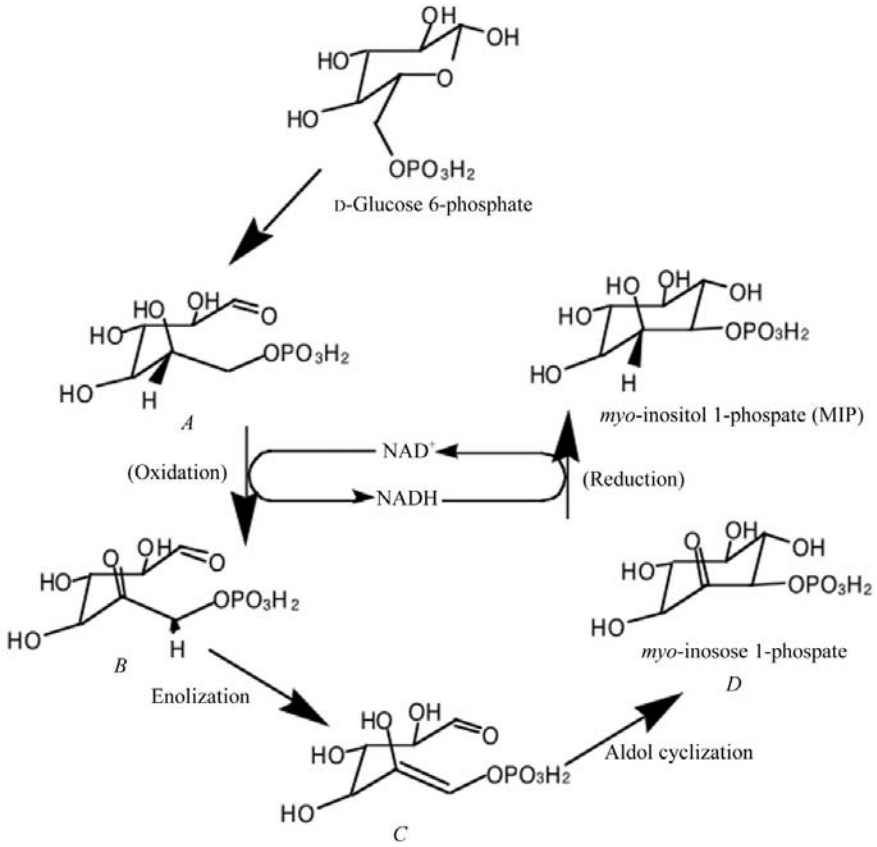

Figure 1
Reaction pathway proposed for MIP synthase.

Table 1
Data collection and refinement statistics.

Values in parentheses denote those values are for the last resolution shell.

	Apo yMIP synthase	yMIP synthase–NAD^+ complex	yMIP synthase–NAD^+ complex	yMIP synthase–NADH complex	yMIP synthase–NADH–EDTA complex
Resolution (Å)	2.6	1.95	2.4	1.7	2.1
Total No. of reflections	44160	214444	56444	160868	161339
Completeness (%)	98.3 (96.8)	96.6 (99.2)	99.7 (100.0)	84.4 (69.5)	99.8 (99.6)
R_{sym}† (%)	12.0 (60.5)	6.4 (42.2)	9.9 (45.3)	7.4 (25.6)	6.7 (42.2)
$I/\sigma(I)$	11.6 (1.9)	23.5 (2.5)	28.6 (3.0)	36.8 (4.4)	31.8 (3.2)
Space group	*C*2	$P2_1$	*C*2	*C*2	*C*2
Unit-cell parameters					
a (Å)	153.54	90.79	152.38	149.86	151.98
b (Å)	97.06	185.58	97.34	99.85	97.61
c (Å)	122.06	94	122.88	122.57	121.72
β (°)	125.72	114.77	126.53	126.64	126.15
R/R_{free}‡ (%)	19.0/27.8	20.8/24.9	20.9/28.8	16.5/19.0	20.9/26.1
Average *B* factor (Å^2)	47	49.6	58.8	22	43.4
No. of water molecules	133	1529	160	1068	180
R.m.s.d. bond lengths (Å)	0.0072	0.0072	0.0078	0.0053	0.0072
R.m.s.d. bond angles (°)	1.39	1.26	1.36	1.35	1.30

† $R_{sym} = \sum \big||I| - |\langle I\rangle|\big| / \sum |I|$, where I is the observed intensity and $\langle I\rangle$ is the average intensity obtained from multiple observations of symmetry-related reflections. ‡ $R = \sum \big||F_{obs}| - |F_{calc}|\big| / \sum |F_{obs}|$; $R_{free} = \sum \big||F_{obs}| - |F_{calc}|\big| / \sum |F_{obs}|$ where reflections belong to a test set of 10% randomly selected data.

lizing the developing negative charge on the enolate O atom. The structure of *Mycobacterium tuberculosis* MIP synthase (Tb MIP synthase) bound to NAD^+ has also recently been reported and a position for a Zn^{2+} ion proposed (Norman *et al.*, 2002). However, the Zn^{2+} ion appears to be located between the amide of the nicotinamide and the nicotinamide phosphodiester on NAD^+. Though apparently not in a position to be directly involved in catalysis, this Zn^{2+} ion chelates a water molecule located very near the putative ammonium ion in the yMIP synthase structure. The nicotinamide is moved significantly from its position in the yMIP synthase structure, as a direct hydrogen bond is observed between the amide and nicotinamide phosphodiester in both published yMIP synthase structures. In addition, several amino acids are also disordered in this structure in the vicinity of the active site that correspond to most of the residues that are disordered in the yMIP synthase/low-occupancy NAD^+ structure.

To determine the relative importance of NAD^+ in the ordering of the active site of yMIP synthase, we have determined the structures of yMIP synthase both completely devoid of NAD^+ and completely occupied with NAD^+. We also present a structure of yMIP synthase bound to NADH at 1.7 Å resolution. This is by far the highest resolution structure of yMIP synthase to date and also contains several provocative differences in the active site relative to the other yMIP synthase structures.

2. Experimental procedures

2.1. Crystallization and data collection

yMIP synthase was purified as previously reported (Stein & Geiger, 2000, 2002). Protein used to grow the *C*2 crystal form of the yMIP synthase–NAD^+ complex, the yMIP synthase–NADH complex, the yMIP synthase–NADH–EDTA complex and apo yMIP synthase was then treated with activated charcoal for 30 min at 277 K to remove cofactors. Crystals of apo yMIP synthase were then grown using the same conditions used to grow the low-occupancy NAD^+–MIP synthase complex and the dgtolP–NAD^+–MIP synthase complex crystals (Stein & Geiger, 2000, 2002). Crystals were then soaked in either NAD^+ or NADH-containing mother liquor (5% PEG 8000, 0.1 *M* NaOAc pH 4.5, 1 m*M* NAD^+ or NADH, respectively) for 12 h. For the yMIP synthase–NADH–EDTA complex crystals, pre-grown apo yMIP synthase crystals were soaked in a stabilizer containing 5 m*M* EDTA in addition to 1 m*M* NADH for 12 h. For the $P2_1$ crystal form of the NAD^+-bound MIP synthase, protein was not treated with activated charcoal before crystallization. For data collection, a single crystal was transferred to cryoprotectant stabilizing solution (5% PEG 8000, 0.1 *M* sodium acetate pH 4.5, 30% glycerol) and flash-frozen. Data for apo yMIP synthase were collected at 113 K on an R-AXIS IV image-plate system with Cu $K\alpha$ X-rays generated with a Rigaku RU-200 rotating-anode generator operated at 50 kV and 90 mA. Data for the $P2_1$ crystal form of NAD^+-bound MIP synthase were collected at the synchrotron radiation source at BioCARS BM-14, Advanced Photon Source, Argonne National Laboratory. Diffraction data reduction and scaling for apo yMIP synthase and the $P2_1$ crystal form of NAD^+-bound MIP synthase were performed using *DENZO* and *SCALEPACK*, respectively (Otwinowski & Minor, 1997). Data for the *C*2 crystal form of the yMIP synthase–NAD^+ complex, the yMIP synthase–NADH complex and the yMIP synthase–NADH–EDTA complex crystals were collected at the synchrotron radiation source at IMCA-CAT ID-17, Advanced Photon Source, Argonne National Laboratory. Diffraction data reduction and scaling were performed using *HKL*2000 (Table 1).

2.2. Structure determination and refinement

For the $P2_1$ crystal form of the yMIP synthase–NAD^+ complex, the structure was solved by molecular replacement using *AMoRe* (Navaza, 1994). A monomer of the yMIP synthase–NAD^+–dgtolP complex (Stein & Geiger, 2002) was used as the search model. Structures of apo yMIP synthase, the *C*2 form of the yMIP synthase–NAD^+ complex, the yMIP synthase–NADH complex and the yMIP synthase–NADH–EDTA complex were solved using the same structure (Stein & Geiger, 2002) as an initial phasing model. The electron-density

maps were traced using *TURBO-FRODO* and multiple rounds of refinement were conducted using *CNS* (Brünger *et al.*, 1998). Data collection and final refinement statistics are tabulated in Table 1. For apo yMIP synthase, the final model contains residues 10–351 and 376–533. The $P2_1$ form of the yMIP synthase–NAD^+ complex model contains residues 10–361 and 380–533 in the *A* and *B* molecules, residues 10–464 and 472–533 in the *C* molecule, and residues 10–362, 380–390 and 410–533 in the *D* molecule. The *C*2 form of the yMIP synthase–NAD^+ complex final structure contains residues 10–362 and 376–533. The yMIP synthase–NADH complex final model contains residues 10–533. The yMIP synthase–NADH–EDTA complex final model contains residues 10–533 in the *A* molecule and 10–371, 376–464 and 472–533 in the *B* molecule. Residues 465–471 of the *B* molecules in all *C*2 structures and of the *B* and *C* molecules in the $P2_1$ structure are also disordered. The final refinement parameters are listed in Table 1.

3. Results and discussion

3.1. The structure of apo yMIP synthase

The 2.6 Å apo yMIP synthase structure is for the most part very similar to the low-occupancy NAD^+–yMIP synthase structure except that several of the previously disordered residues are now well visualized in the electron-density map. The flexible strand (β15 as defined in the original yMIP synthase crystal structures; Stein & Geiger, 2002) is ordered in this structure, although the rest of the mobile region is still disordered. The conformation of this strand encompassing residues 391–408 is very similar to that seen in the yMIP synthase–NAD^+–dgtolP structure. As expected, no density for NAD^+ is evident in either of the two molecules in the asymmetric unit, confirming that charcoal treatment fully removes residual NAD^+ from the enzyme. In addition, the loop from residues 194–198 is in a similar conformation to that seen in the NAD^+/dgtolP-bound structure as opposed to the low-occupancy NAD^+-bound structure. Those residues in the active site that are ordered in this structure (Ser323, Gln325, Lys412, Asp438 and Lys489) are in very similar locations to those seen in the previous yMIP synthase structures. The overall structure of the apo yMIP synthase is very similar to all other structures of yMIP synthases, with all three domains overlaying well with the other structures (r.m.s.d.s of 0.9 and 1.0 Å between the NAD^+-bound yMIP synthase and NADH-bound yMIP synthase, respectively). These observations lead to the conclusion that while the active site of MIP synthase is very flexible, its NAD^+-binding domain is very rigid. It is also evident that a smaller region of the protein depends on substrate binding for folding than was first thought, as the β15 strand encompassing amino acids 396–406 is well ordered in the absence of an inhibitor or substrate molecule. However, the active site is still left quite exposed, as the front helix α14 is disordered.

3.2. The structure of the yMIP synthase–NAD^+ complex

We have produced two distinct crystal forms of the yMIP synthase–NAD^+ complex, a *C*2 crystal form, which is essentially identical to the crystal form of the rest of yMIP synthase structures, and a $P2_1$ form (Table 1). The $P2_1$ form contains an entire tetramer in the asymmetric unit. Both crystal forms are obtained by soaking apo yMIP synthase crystals with 1 m*M* NAD^+; neither crystal form grows in the presence of NAD^+. Overall, all the NAD^+-bound structures are very similar (r.m.s.d.s are in the region of 0.9 Å between each of the six independent molecules in the two crystal forms). As expected, NAD^+ is fully occupied in these structures. The adenine, adenine ribose and both phosphodiesters are well ordered and are 100% occupied. The conformation of NAD^+ is very similar to that seen in the published low-occupancy NAD^+–yMIP synthase structure, with a hydrogen bond formed between the amide N atom of the nicotinamide and a phosphodiester O atom (Fig. 2). This hydrogen bond serves to pinch the phosphate and nicotinamide together, dictating the sugar pucker of the intervening ribose. The residues involved in NAD^+ binding are fairly well conserved across the species, although the conservation is not complete. The loop between β3 and α1 (Ile71–Gly78) plays an important role in NAD^+ binding, similar to that observed for other NAD^+-binding proteins. Virtually all of these residues make direct interactions with

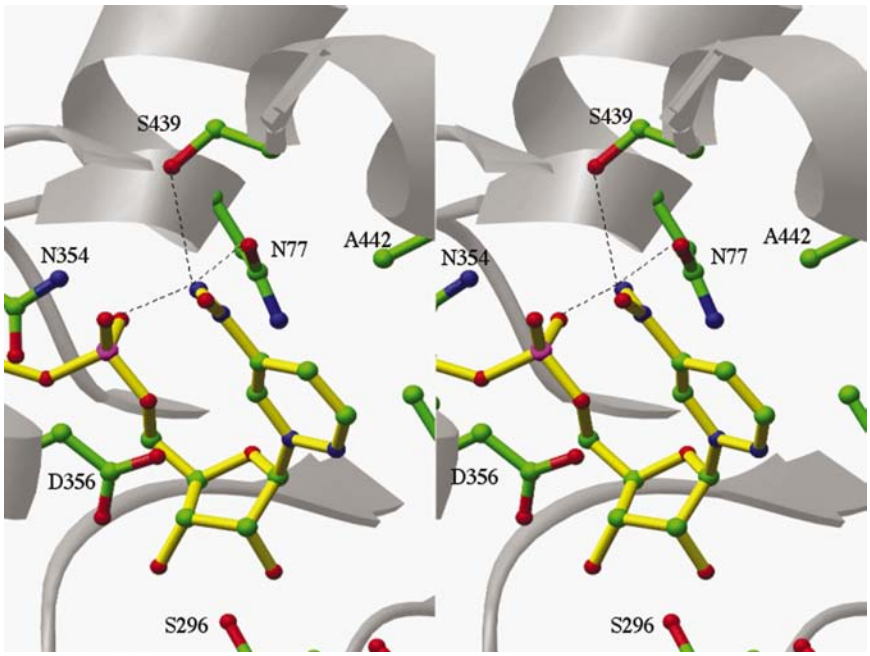

Figure 2
Stereoview of the hydrogen bond that stabilizes the conformation of NAD^+. In addition to the phosphodiester oxygen, the nicotinamide nitrogen also makes hydrogen bonds with Ser439 O and Asn77 O.

NAD^+ and constitute the largest cluster of residues that interact with the cofactor. The adenine portion of NAD^+ is completely engulfed by the second insertion in the Rossmann fold that encompasses amino acids 153–214 and makes interactions with several hydrophobic residues including Ile71, Gly72, Trp147, Ile149, Ile185, Ala245 and Pro277. It also makes tight hydrogen bonds between N1 and Ser184 OG and N6 and Ile185 O (both less than 3.0 Å). This elaborate hydrophobic and hydrogen-bonding network between the adenine portion of NAD^+ and the enzyme is probably largely responsible for the increased binding constant (K_M = 0.017 m*M*) of MIP synthase when compared with enzymes that use NAD^+ as a substrate. Overall, 1054 $Å^2$ of surface area are buried in the interaction of yMIP synthase with NAD^+.

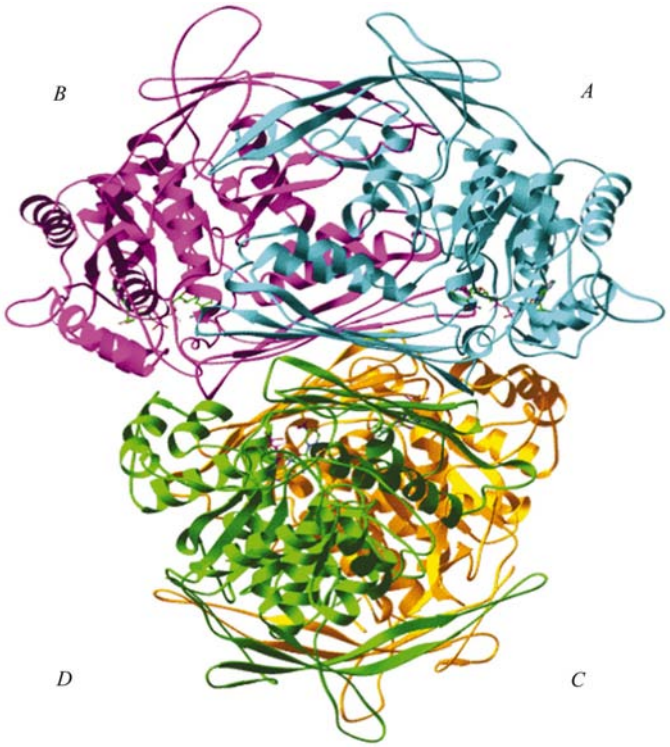

Figure 3
The entire tetramer of the $P2_1$ structure of the MIP synthase–NAD^+ complex. Molecule *A* is colored cyan, *B* magenta, *C* gold and *D* green.

In the *C*2 crystal form, both molecules in the asymmetric unit are very similar and both show that most of the 60 residues found to be disordered in the original published structure are disordered in this structure as well. This is especially true of the helix that covers the front of the active site (α14) including amino acids 362–379. This helix is completely disordered in both of the molecules in the asymmetric unit. Although there is some scattered density for the flexible strand (β15), it too is for the most part disordered in this structure as well.

The situation is more complex in the $P2_1$ crystal form. This crystal form contains four independent molecules in the asymmetric unit, each in a different crystal-packing environment. Significant variation is evident in the four molecules, especially with regard to the active-site residues. The molecules are arranged with molecules *A* and *B* forming one dimer and molecules *C* and *D* the other. The two dimers are related by a non-crystallographic twofold axis that runs between the β-sheets that make up the floor domain. Molecule *A* is related to molecule *C*, while molecule *B* is related to *D* by this twofold axis (Fig. 3). Molecules *A*, *B* and *D* are similar, with the region encompassing amino acids 361–380 (α14 plus some of α15) completely disordered in these structures. The position of the putative ammonium ion in the previously published structure of the yMIP synthase–NAD^+–dgtolP complex (Stein & Geiger, 2002) is occupied in these molecules and coordinated by Asn354, Asp356 and Asp438, with Asp356 swinging into the position of the dgtolP phosphate. In all three of these molecules (molecules *A*, *B* and *D*) density for the mobile strand (β15) is very poor but indicative of at least partial occupancy of this strand, as removal of it results in significant positive density in the $F_o - F_c$ map in this region. This is more or less similar to that seen in the *C*2 crystal form. The increased order of this strand in the apo structure *versus* these NAD^+-bound structures is puzzling, but is borne out in the data.

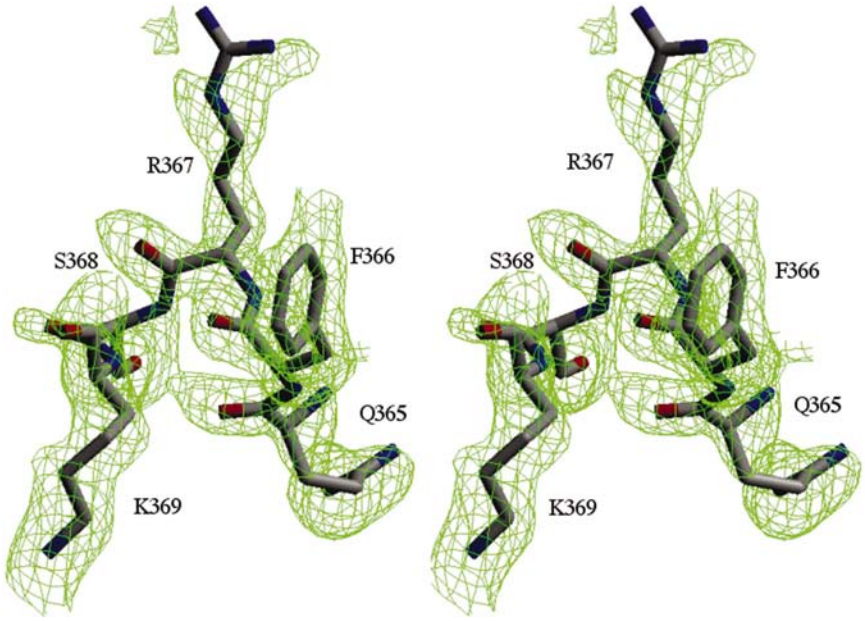

Figure 4
The $F_o - F_c$ electron-density map of the active site of molecule *C* in the $P2_1$ structure of the MIP synthase–NAD^+ complex contoured at 1.8σ; residues 365–369 are shown.

In contrast, molecule *C* in the $P2_1$ crystal form provides a surprising result in that the entire mobile domain has become ordered; though the density for some regions is not complete. Fig. 4 shows the $F_o - F_c$ map of

this region. Most of the active-site residues occupy similar positions to those seen in the yMIP synthase–NAD^+–dgtolP complex. These include Ser323, Asn354, Lys369, Lys412, Asn438 and Lys489. On the other hand, Asp356, which was flipped out of the active site in the dgtolP complex, is now flipped into the active site, occupying the position of the inhibitor dgtolP phosphate and coordinating a feature occupied by the position of the putative ammonium ion. This residue replaces one of the coordination sites occupied by the inhibitor phosphate by the putative ammonium ion. Gln325, which was implicated in substrate binding when the substrate was modeled in a pseudocyclic conformation consistent with aldol cyclization, has also moved and now makes a hydrogen bond with Lys412, buttressing its orientation in the active site. The fact that such changes in the active site can occur may indicate that there are significant differences in the conformation of the amino acids in the active site upon bona fide substrate binding, calling into question some of the details of the original model proposed for the reaction. The reason why the molecule *C* active site is better ordered than in any of the other yMIP synthase–NAD^+ complex molecules seen crystallographically is unclear. However, a significant electron-density feature is present in the center of the active site, overlapping the position of the inhibitor in the yMIP synthase–dgtolP–NAD^+ structure. This indicates that the active site of molecule *C* is at least partially occupied by a small molecule that is contributing to the stabilization of the region. The fact that other small molecules can be bound in the active site will be borne out in the yMIP synthase–NADH complex structure described below.

The conclusion to be drawn from the sum of these structures is that the active site of yMIP synthase is indeed quite flexible, with the front helix (α14) of the active site encompassing residues 362–374 disordered in the absence of a bound substrate, inhibitor or other small molecule in the active site. Helix α13, encompassing residues 352–360, is to some extent ordered to allow interaction between this helix and NAD^+. The remainder of the flexible region, encompassing residues 375–408, can be discerned in most of the structures whether NAD^+ is bound or not, but the residues are significantly less

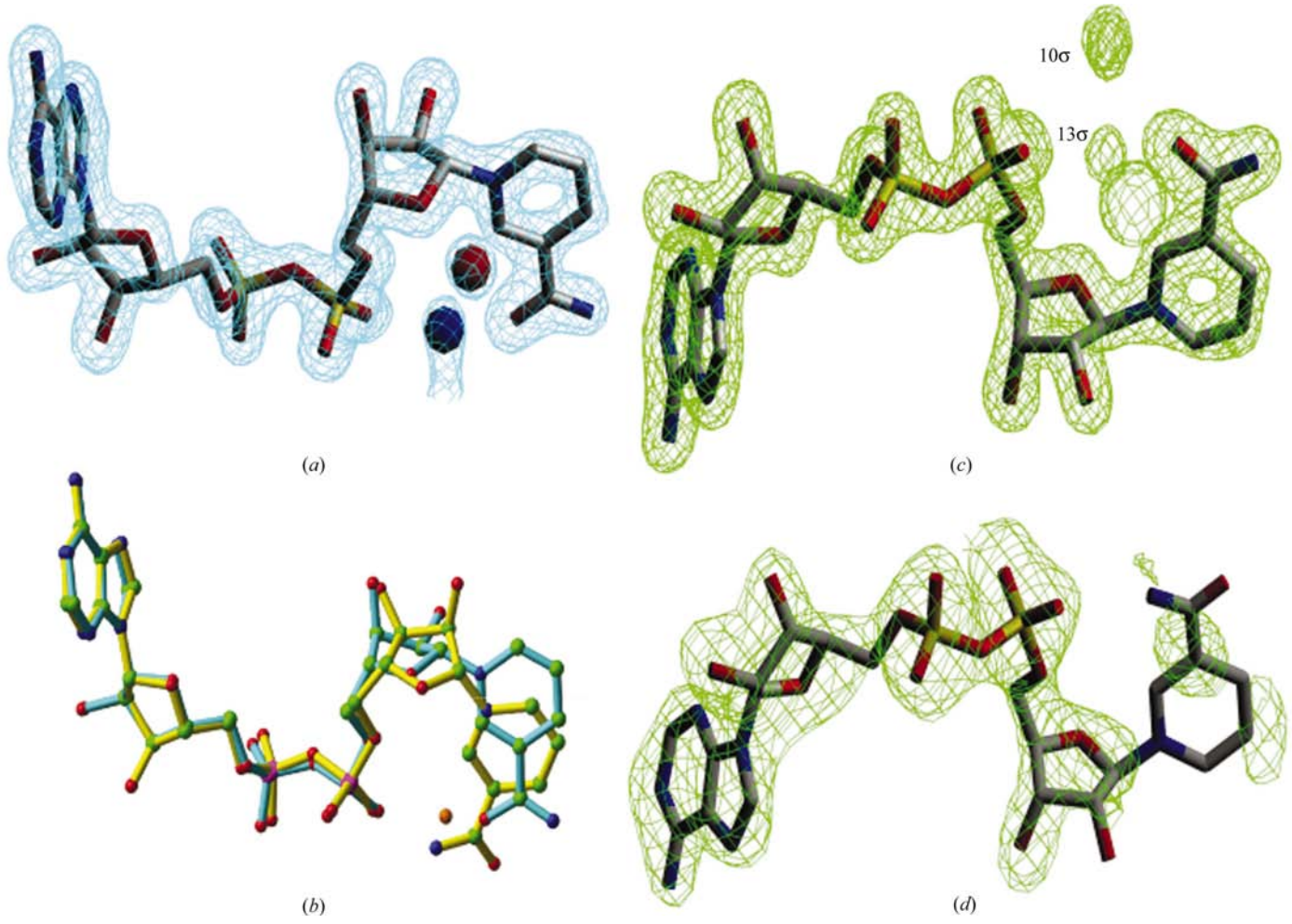

Figure 5
(*a*) The $2F_o - F_c$ electron-density map of the MIP synthase–NADH complex structure contoured at 2.4σ around the NADH. The putative divalent cation is shown in blue; in red is a water molecule that coordinates to the divalent cation. (*b*) Overlay of cofactors in the NAD^+-bound structure in yellow and the NADH-bound structure in cyan. (*c*) Simulated-annealing omit electron-density map of the MIP synthase–NADH complex structure contoured at 5σ. (*d*) Simulated-annealing omit electron-density map of the MIP synthase–NADH–EDTA complex structure contoured at 1.8σ.

ordered in the NAD^+-bound molecules than they are in the apo structure in the absence of binding by inhibitor, substrate or other small molecule.

3.3. The 1.7 Å structure of the yMIP synthase–NADH complex

When the apo yMIP synthase crystals were soaked in an NADH-containing stabilizer, several provocative differences were observed in the structure. Firstly, the quality of the crystal improved significantly, with diffraction evident to 1.6 Å. This data produced a spectacular electron-density map, with obvious holes even in the five-membered ribose rings of NADH (Fig. 5*a*). The refinement of this structure currently has an R factor of 16.5% with an $R_{\rm free}$ of 19%. For the most part, the structure is similar to all the other known yMIP synthase structures [the r.m.s.d. between the structure of the MIP synthase–NADH complex (molecule *A*) and molecule *A* of the $P2_1$ structure of the MIP synthase–NAD^+ is 1.15 Å, and the r.m.s.d. between the structure of the MIP synthase–NADH complex and molecule *A* of the *C*2 structure of the MIP synthase–NAD^+ is 0.83 Å]. However, there are also several obvious differences in the structure. The nicotinamide ring of NADH moves away from the phosphodiester in this structure, eliminating the hydrogen bond between the amide N atom and the phosphodiester O atom (Fig. 5*b*). In the NAD^+-bound structure, the positively charged N1 of nicotinamide makes a polar interaction with Asp356 OD1, but this interaction seems to disappear in the NADH-bound structure. In fact, there is a 13σ peak of electron density between the nicotinamide and the phosphodiester O atom (Fig. 5*c*). This feature coordinates both the nicotinamide amide and the phosphodiester oxygen, but with interatomic distances that are relatively short for hydrogen bonds (2.34 and 2.36 Å, respectively). These distances are perhaps more compatible with a metal ion than a hydrogen-bonding species. Modeling this feature as an Mg^{2+} cation accounts for the density rather well, although the coordination distances are a little long for Mg^{2+} (typical Mg—O distances are 2.1–2.3 Å in protein structures). On the other hand, both Zn^{2+} and Mn^{2+} model the feature poorly, as the coordination bond lengths are longer than expected (Zn—O distances are typically between 1.8 and 2.1 Å in various protein structures). Either Zn^{2+} or Mn^{2+} positioned at this location resulted in significant negative density in the $F_o - F_c$ map, indicating both to be too electron-rich to account for the feature. When the apo MIP synthase crystals were soaked in EDTA in addition to NADH, all the active-site residues are ordered as in the MIP synthase–NADH structure, with the exception of residues 372–375 in molecule *B*. However, the conformation of the nicotinamide is completely different from that of the NADH-bound structure; in fact, it is similar to that of the NAD^+-bound structure. Importantly, the electron-density feature between the nicotinamide and phosphodiester has disappeared (Fig. 5*d*), indicating that this is indeed a divalent cation. However, it is still unclear which specific divalent cation this is. The density of the nicotinamide is also much worse, indicating increased mobility of the nicotinamide ring in the absence of a putative divalent cation. This feature is coordinated to two other features in the map, one of which is very close to the position of the putative ammonium ion described in the dgtolP complex.

The coordination geometry about this putative metal is tetrahedral, with bond angles ranging from 101 to 107°. Both the conformation of the NADH and the location of this possible metal ion are similar to that seen in the Tb structure (Norman *et al.*, 2002), where a Zn^{2+} ion was modeled at this position (Fig. 6). However, the coordination about the putative metal ion is different in the Tb structure in that the distances between the ion and the two NAD^+ ligands are shorter (2.08 and 2.16 Å) and an absolutely conserved serine residue Ser311, which is conserved as Ser439 in yMIP synthase, is the fourth ligand and also has a relatively short (2.42 Å) distance to the putative metal ion. In our structure, Ser439 is moved about 2 Å away from this site (Norman *et al.*, 2002). Instead, the fourth coordination is occupied by another significant feature (10σ in the $F_o - F_c$ electron-density map) that is also about 2.29 Å away from the putative metal. Importantly, Ser439 is identically positioned in all structures of yMIP synthase determined so far. The position of the putative

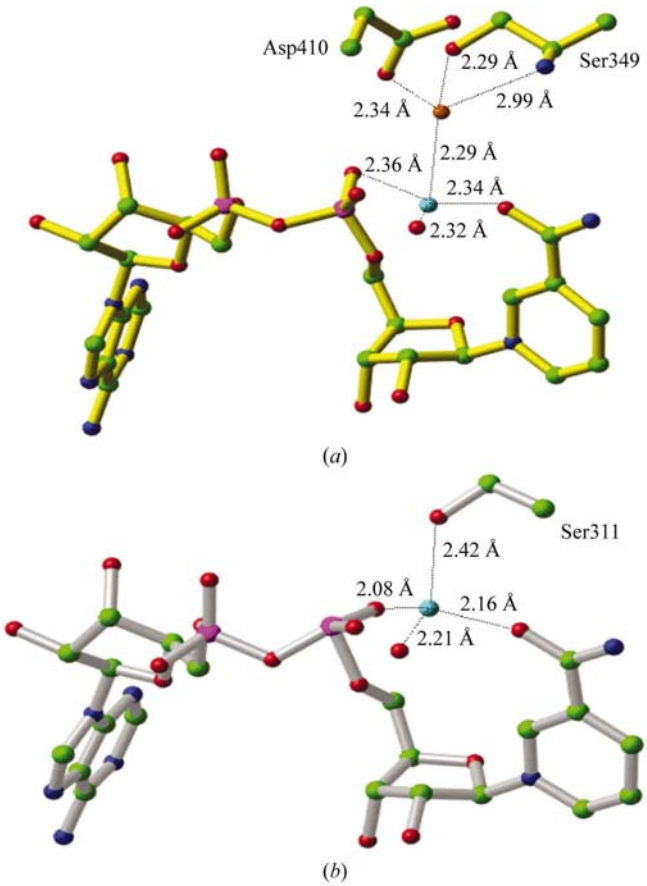

Figure 6
(*a*) The NADH-bound MIP synthase from *S. cerevisiae*. The modeled putative divalent cation is shown in cyan, the fourth ligand of the putative divalent in orange and the conserved water molecule in red. (*b*) The NAD^+-bound MIP synthase from *M. tuberculosis*; the Zn^{2+} is in cyan (Norman *et al.*, 2002).

metal relative to the nicotinamide ring would seem to preclude it being directly involved in any chemistry. Previous experiments performed on yMIP synthase have ruled out the direct involvement of a divalent cation (Mauck *et al.*, 1980; Pittner & Hoffmann-Ostenhof, 1976, 1978). This putative divalent cation bridges the cofactor and thus might bring the nicotinamide C4 close to the substrate oxidation center C5. It also coordinates an important water molecule that makes hydrogen bonds with two absolutely conserved aspartate residues, Asp356 and Asp438. It may influence the pK_a of the acidic side chains of Asp356 and Asp438.

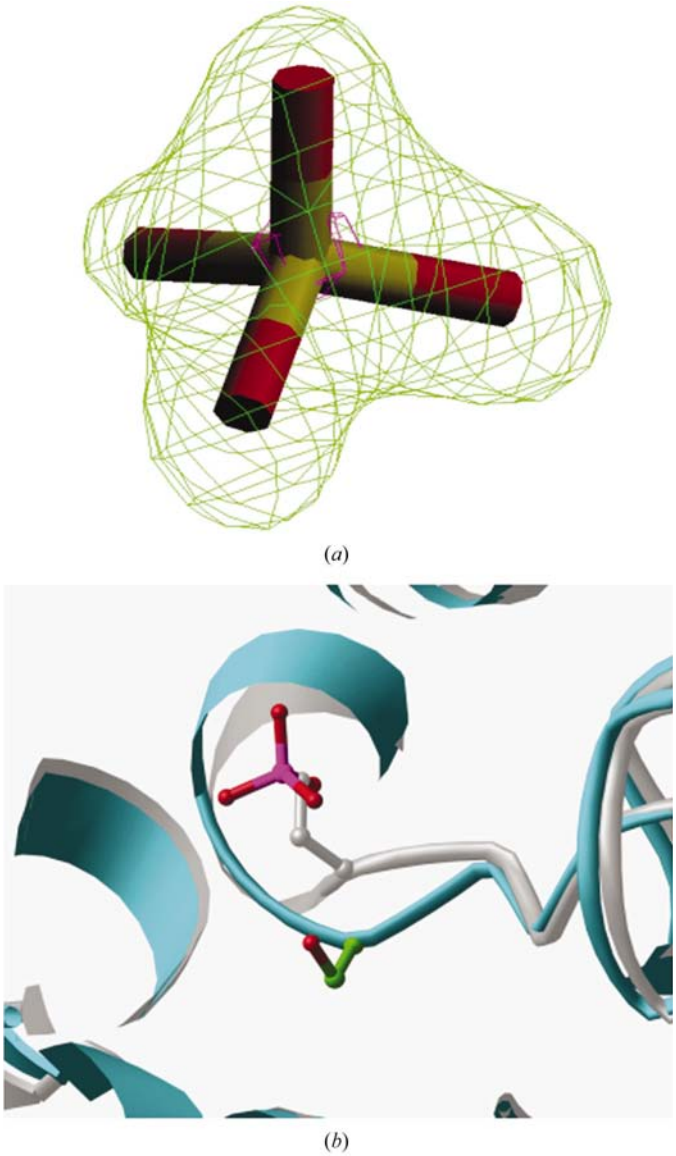

Figure 7
(*a*) Simulated-annealing omit electron-density map of MIP synthase–NADH active site with a phosphate modeled in. The 7σ contour level is shown in green and the 20σ contour level in magenta. (*b*) The motion of Ser323-Gly324-Gln325-Thr326 loop owing to phosphate binding in the NADH-bound structure. The NAD^+-bound structure is in silver while the NADH-bound structure is in cyan. The phosphate found in the NADH-bound structure is shown and colored by atom type (red, oxygen; pink, phosphorus).

Significant structural changes are also evident on the opposite side of the active site. Most obviously, all of the residues in the mobile region are very well ordered and two small molecules are bound in the active site of the enzyme. The $F_o - F_c$ density for both of these molecules is more than 7σ in our refined maps. One of these molecules is clearly a tetrahedron of heavy atoms consistent with either a sulfate or phosphate ion. We have tentatively assigned this density to be phosphate and Fig. 7(*a*) shows a phosphate molecule fitted to the 7σ $F_o - F_c$ map. In fact, the position of the phosphorus coincides with a 22σ peak in the $F_o - F_c$ map. As shown, the density is quite consistent with a phosphate moiety. A significant conformational change has occurred to accommodate this phosphate in that Ser323 has moved more than 4 Å and is now pointing out of the active site. The position of Ser323 is similar to that seen in the Tb structure, where Ser200 occupies a similar position. However, this conformation is distinct from virtually all other yMIP synthase structures so far determined, including apo, dgtolP/NAD^+-bound and NAD^+-bound structures (Fig. 7*b*). Consistent with the identification of this feature as anionic, the putative phosphate makes salt-bridge interactions with three absolutely conserved lysine residues, namely Lys373, Lys412 and Lys489. It additionally makes hydrogen bonds with the main-chain N atoms of Gly324, Gln325 and Thr326. Both Gln325 and Lys373 adopt different conformations relative to the other yMIP synthase structures to position themselves to make these interactions. While Gln325 is not conserved among bacterial MIP synthases (Ala204 in the Tb structure), Lys373, Ser323 and Lys489 are completely conserved in all MIP synthases and are in very similar positions in the Tb structure to that seen in the yMIP–NADH complex structure. This phosphate position is far from that of the yMIP synthase–dgtolP complex structure. In fact, it is on the opposite side of the active site from that of the dgtolP phosphate group. The only other significant change in the active site involves Cys436, a residue conserved in all eukaryotic MIP synthases but not in the bacterial enzymes (Val308 in the Tb enzyme). While Cys436 is basically positioned out of the active site in all other yMIP synthase structures, it is flipped into the active site in the yMIP–NADH structure.

In addition to the putative phosphate in the active site, there is another 5σ electron-density feature in the $F_o - F_c$ map of this structure. We have tentatively modeled a molecule of glycerol into this density. We chose glycerol based on the shape and size of the density and the fact that glycerol was used as the cryoprotectant when freezing these crystals. The putative glycerol molecule is in a similar position to the dgtolP inhibitor found in the previous structure of the yMIP synthase–NAD^+–dgtolP complex. It makes numerous interactions with active-site residues, namely Asn350, Leu352, Asn356, Leu360, Lys369, Lys373, Ile402, Lys412 and Asp438. It is also positioned above the C4 carbon of the nicotinamide from which the oxidation and reduction steps occur. Fig. 8 shows the putative phosphate and glycerol molecule within the active site of the enzyme. Apparently, the active site is ordered in this structure owing to binding of the two small molecules within it. It is important to realise that the active

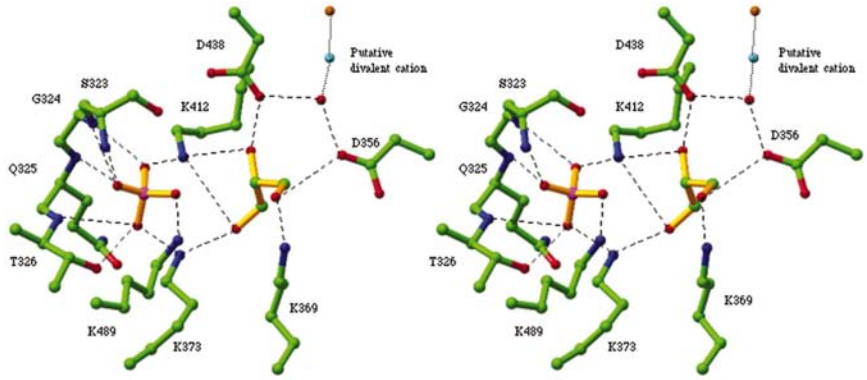

Figure 8
Interactions observed between the MIP synthase active-site residues and the modeled phosphate and glycerol molecules.

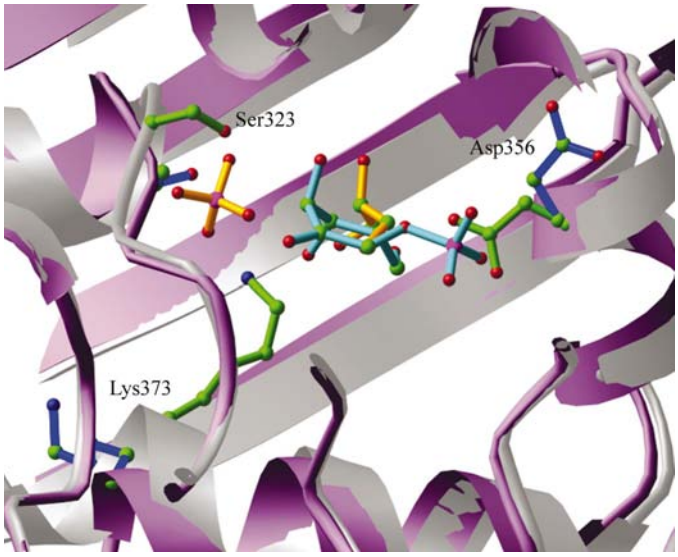

Figure 9
Overlay of the MIP synthase–NADH complex structure in silver and the MIP synthase–NAD^+–2-deoxy-D-glucitol 6-phosphate complex structure (Stein & Geiger, 2002) in lavender. The phosphate and glycerol in the NADH-bound structure are shown in gold, 2-deoxy-D-glucitol 6-phosphate in the previous inhibitor-bound structure in cyan, side chains of the NADH-bound structure in green and side chains of the previous inhibitor-bound structure in blue.

site of yMIP synthase is completely ordered only when small molecules are bound there. Those structures, whether with or without NAD^+ or NADH, that do not have small molecules bound show disorder in the active-site region that allows the access of the substrate. Therefore, all of these structures are consistent with the idea that the substrate reorders the active site, thereby encapsulating itself within the enzyme.

This structure also calls into question the mechanism proposed based on the dgtolP complex structure (Stein & Geiger, 2002) (Fig. 9). As we clearly see a phosphate-like anion bound on the opposite side of the active site, an important question arises as to which phosphate-binding site is occupied during the intramolecular aldol cyclization. The modeling that gave rise to this mechanism assumed the phosphate position to be invariant and all modeling was based on this assumption. If the phosphate is actually bound on the opposite side of the active site, a complete rethinking of the mechanism will be required. Interestingly, it is possible to position a substrate in the active site based on the position of the phosphate in the yMIP synthase–NADH structure and the position of the putative glycerol moiety.

These new results introduce many new questions regarding the mechanism of yMIP synthase and also, by extension, the mechanism of other MIP synthases. The change in position of the nicotinamide, the various changes in conformation in the active site and the possible presence of a metal ion all may lead to a rethinking of the proposed mechanism of the enzyme. The mechanistic role of this putative metal ion is not clear at this point. It is worthwhile to note that though the *A. fulgidus* enzyme has been shown to require divalent ions such as Zn^{2+} or Mn^{2+} for activity (Chen *et al.*, 2000), it is therefore possible that the *A. fulgidus* enzyme also has a distinctly different structure.

3.4. Comparison of the structures of yMIP synthase and Tb MIP synthase

Although the active sites of the yMIP synthase–NADH complex and the Tb MIP synthase–NAD^+ complex are similar in many regards, there are several notable differences between the two enzymes (Norman *et al.*, 2002). The Tb enzyme is considerably shorter, with only 367 amino acids compared with 533 amino acids for yMIP synthase. Most of these amino acids correspond to the N-terminus of yMIP synthase, which constitutes a 62-amino-acid domain containing two long β-strands (β1 and β2). The Tb enzyme, on the other hand, lacks this domain and begins with the Rossmann-fold domain. In addition, significant parts of all three Rossmann-fold insertions are also missing. In contrast to yMIP synthase, the first insertion does not impinge on the central domain, simply forming a 19-amino-acid loop that extends away from the structure. Fully 13 amino acids of this insertion make interactions across the dimer interface in yMIP synthase, all of which are lost in the Tb MIP synthase structure. Most of the second domain is present in the Tb structure and serves to completely engulf the adenine ring of NAD^+ as it does in yMIP synthase, although only 44 of the 61 residues are present in Tb MIP synthase. The third insertion, which consists of a helix and two loops located on the surface of the Rossmann-fold domain in yMIP synthase, is essentially missing in the Tb MIP synthase structure. In addition, the C-terminus of yMIP synthase is missing from Tb MIP synthase. This region also makes a large number of interactions across the dimerization interface of the enzyme. Taken together, the Tb enzyme has a significantly less elaborate dimerization interface than yMIP synthase, involving only a helix and a strand (α12 and β17, respectively; yMIP synthase numbering) of the floor domain.

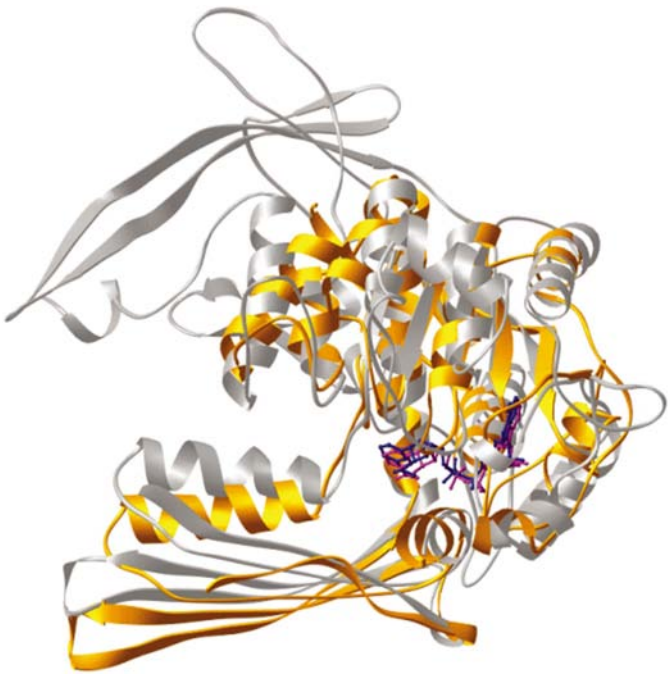

Figure 10
Overlay of the yMIP synthase–NADH complex structure (silver) and the Tb MIP synthase structure (gold); NAD^+ molecules are shown in blue for yMIP synthase and in magenta for Tb MIP synthase.

However, the dimerization interface is very similar in the two molecules in this region. Virtually all of the residues in Tb MIP synthase that are involved in the interface also interact in yMIP synthase, although many are not conserved. Indeed, when the structures are aligned using only residues from the floor domain, the structures align, as does the dimerization interface, with an r.m.s.d. of 3.5 Å between the two structures for the overlay of just this domain.

Two residues in Tb MIP synthase, Phe295 and Arg218, were found to be inserted into corresponding cavities in the opposing monomer (Norman *et al.*, 2002). Phe295 is located in the floor domain of the enzyme, is conserved in yMIP synthase and also makes very similar interactions in the yeast enzyme. Arg218, on the other hand, is one of the few residues in the Rossmann-fold domain that is involved in the dimerization interface and it is not conserved in yMIP synthase (the equivalent residue is Ala339 in yMIP synthase). The result of this dramatic change is to create significant space between the two domains. The result is that Tyr486 and Trp487 move significantly to fill the void. Thus, Tyr486 from the adjacent monomer (Tyr343 in Tb MIP synthase) makes an interaction with the equivalent residue in both structures (Arg218 in Tb MIP synthase and Ala339 in yMIP synthase), but it has to move more than 7 Å to do so. This structural change appears to have a profound effect on the relative orientation of the two domains (Fig. 10). As shown in Fig. 10, when the Rossmann-fold domains of Tb and yMIP synthase are aligned (giving an r.m.s.d. of 2.5 Å) a significant difference in the position of the floor domain is evident. The motion can be characterized as a hinge motion centered at the region where Arg218 is changed to Ala338 in yMIP synthase. It is this Arg to Ala change and the corresponding structural change that accompanies it that seem to be the most directly responsible for the hinge movement of the two domains. In addition, a two-amino-acid insertion, Gln201 and Val202, in Tb MIP synthase also contributes to the differences in the structure of this region. Significantly, essentially all of the interactions here are across the dimer, not between the two domains of a monomer. It is thus the dimerization interface that determines the relative orientation of the two domains. In spite of this rather large and surprising interdomain motion between the two enzymes, virtually all of the amino acids are in very similar locations within the active sites of the two enzymes as discussed above. This is because the active site is very near the center of the hinge motion and therefore does not undergo as significant an interdomain motion as the part of the molecule that is furthest from the hinge. In spite of this change in the relative orientation of the two domains in the two structures, the preponderance of evidence at present suggests that yMIP synthase does not undergo hinge motion upon binding of the substrate or inhibitor, since all structures of yMIP synthase, whether inhibitor-bound, apo, NAD^+-bound or bound by NADH, phosphate and glycerol, have identical interdomain orientations. However, it may be possible that such an interdomain motion may occur for regulatory or other reasons.

Data were collected at the beamline 17-ID in the facilities of the Industrial Macromolecular Crystallography Association Collaborative Access Team (IMCA-CAT) at the Advanced Photon Source, Argonne National Laboratory. These facilities are supported by the companies of the Industrial Macromolecular Crystallography Association through a contract with Illinois Institute of Technology (IIT), executed through IIT's Center for Synchrotron Radiation Research and Instrumentation. Use of the BioCARS BM-14 beamline at the Advanced Photon Source for data collection was supported by National Institutes of Health, National Center for Research Resources, under grant no. RR07707. Use of the Advanced Photon Source was supported by the US Department of Energy, Basic Energy Sciences, Office of Science under Contract No. W-31-109-Eng-38.

References

Abu-Abied, M. & Holland, D. (1994). *Plant Physiol.* **106**, 1689.
Adhikari, J. & Majumder, A. L. (1983). *FEBS Lett.* **163**, 46–49.
Adhikari, J. & Majumder, A. L. (1988). *Ind. J. Biochem. Biophys.* **25**, 408–412.
Arganoff, B. W. & Fisher, S. K. (1991). In *Inositol Phosphates and Derivatives*, edited by A. B. Reitz. Washington, DC: American Chemical Society.
Barnett, J. E. & Corina, D. L. (1968). *Biochem. J.* **108**, 125–129.
Belmaker, R. H., Bersudsky, Y., Agam, G., Levine, J. & Kofman, O. (1996). *Annu. Rev. Med.* **47**, 47–56.
Belmaker, R. H., Bersudsky, Y., Benjamin, J., Agam, G., Levine, J. & Kofman, O. (1995). In *Depression and Mania: From Neurobiology to Treatment*, edited by G. L. Gessa, W. Fratta, L. Pani & G. Serra. New York: Raven Press.

Berridge, M. J., Downes, C. P. & Hanley, M. R. (1982). *Biochem. J.* **206**, 587–595.
Berridge, M. J. & Irvine, R. F. (1989). *Nature (London)*, **341**, 197–205.
Brünger, A. T., Adams, P. D., Clore, G. M., DeLano, W. L., Gros, P., Grosse-Kunstleve, R. W., Jiang, J. S., Kuszewski, J., Nilges, M., Pannu, N. S., Read, R. J., Rice, L. M., Simonson, T. & Warren, G. L. (1998). *Acta Cryst.* D**54**, 905–921.
Chen, L., Zhou, C., Yang, H. & Roberts, M. F. (2000). *Biochemistry*, **39**, 12415–12423.
Dean-Johnson, M. & Henry, S. A. (1989). *J. Biol. Chem.* **264**, 1274–1283.
Exton, J. H. (1986). *Adv. Cyclic Nucleotide Protein Phosphorylation Res.* **20**, 211–62.
Frey, P. A. (1987). In *Pyridine Nucleotide Coenzymes: Chemical, Biochemical and Medical Aspects*, part B, edited by D. Dolphin. New York: John Wiley & Sons.
Hasegawa, R. & Eisenberg, F. Jr (1981). *Proc. Natl Acad. Sci. USA*, **78**, 4863–4866.
Ishitani, M., Majumder, A. L., Bornhouser, A., Michalowski, C. B., Jensen, R. G. & Bohnert, H. J. (1996). *Plant J.* **9**, 537–548.
Johnson, M. D. (1994). *Plant Physiol.* **105**, 1023–1024.
Johnson, M. D. & Sussex, I. M. (1995). *Plant Physiol.* **107**, 613–619.
Loewus, F. A. & Kelly, S. (1962). *Biochem. Biophys. Res. Commun.* **7**, 204–208.
Loewus, M. W. (1977). *J. Biol. Chem.* **252**, 7221–7223.
Loewus, M. W. & Loewus, F. A. (1973). *Plant Sci. Lett.* **1**, 368–371.
Loewus, M. W. & Loewus, F. A. (1980). *Carbohydr. Res.* **82**, 333–342.
Lohia, A., Hait, N. C. & Majumder, A. L. (1999). *Mol. Biochem. Parasitol.* **98**, 67–79.
Majumder, A. L., Johnson, M. D. & Henry, S. A. (1997). *Biochim. Biophys. Acta*, **1348**, 245–256.
Mauck, L. A., Wong, Y. H. & Sherman, W. R. (1980). *Biochemistry*, **19**, 3623–3629.
Migaud, M. E. & Frost, J. W. (1995). *J. Am. Chem. Soc.* **117**, 5154–5155.
Navaza, J. (1994). *Acta Cryst.* A**50**, 157–163.
Norman, R. A., McAlister, M. S., Murray-Rust, J., Movahedzadeh, F., Stoker, N. G. & McDonald, N. Q. (2002). *Structure*, **10**, 393–402.
Otwinowski, Z. & Minor, W. (1997). *Methods Enzymol.* **276**, 307–326.
Park, D., Jeong, S., Lee, S., Park, S., Kim, J. I. & Yim, J. (2000). *Biochim. Biophys. Acta*, **1494**, 277–281.
Pittner, F. & Hoffmann-Ostenhof, O. (1976). *Hoppe-Seyler's Z. Physiol. Chem.* **357**, 1667–1671.
Pittner, F. & Hoffmann-Ostenhof, O. (1978). *Hoppe-Seyler's Z. Physiol. Chem.* **359**, 1395–1400.
Potter, B. V. L. & Lampe, D. (1995). *Angew. Chem. Int. Ed. Engl.* **34**, 1933–1972.
Sherman, W. R., Loewus, M. W., Pina, M. Z. & Wong, Y. H. (1981). *Biochim. Biophys. Acta*, **660**, 299–305.
Sherman, W. R., Stewart, M. A. & Zinbo, M. (1969). *J. Biol. Chem.* **244**, 5703–5708.
Smart, C. C. & Fleming, A. J. (1996). *Plant J.* **4**, 279–293.
Stein, A. J. & Geiger, J. H. (2000). *Acta Cryst.* D**56**, 348–350.
Stein, A. J. & Geiger, J. H. (2002). *J. Biol. Chem.* **277**, 9484–9491.
Tian, F., Migaud, M. E. & Frost, J. W. (1999). *J. Am. Chem. Soc.* **121**, 5795–5796.
Vaden, D. L., Ding, D., Peterson, B. & Greenberg, M. L. (2001). *J. Biol. Chem.* **276**, 15466–15471.
Wang, X. & Johnson, M. D. (1995). *Plant Physiol.* **110**, 336.
Wong, Y. H., Mauck, L. A. & Sherman, W. R. (1982). *Methods Enzymol.* **90**, 309–314.